Attenuation correction with region growing method used in the positron emission mammography imaging system *

GU Xiao-Yue(顾笑悦)[1,2;1)] LI Lin(李琳)[1,2] YIN Peng-Fei(尹鹏飞)[1,2] YUN Ming-Kai(员明凯)[1,2]
CHAI Pei(柴培)[1,2] HUANG Xian-Chao(黄先超)[1,2] SUN Xiao-Li(孙校丽)[1,2] WEI Long(魏龙)[1,2]

[1] Key Laboratory of Nuclear Radiation and Nuclear Energy Technology, Institute of High Energy Physics, Chinese Academy of Sciences, Beijing 100049, China
[2] Beijing Engineering Research Center of Radiographic Techniques and Equipment, Beijing 100049, China

Abstract: The Positron Emission Mammography imaging system (PEMi) provides a novel nuclear diagnosis method dedicated for breast imaging. With a better resolution than whole body PET, PEMi can detect millimeter-sized breast tumors. To address the requirement of semi-quantitative analysis with a radiotracer concentration map of the breast, a new attenuation correction method based on a three-dimensional seeded region growing image segmentation (3DSRG-AC) method has been developed. The method gives a 3D connected region as the segmentation result instead of image slices. The continuity property of the segmentation result makes this new method free of activity variation of breast tissues. The threshold value chosen is the key process for the segmentation method. The first valley in the grey level histogram of the reconstruction image is set as the lower threshold, which works well in clinical application. Results show that attenuation correction for PEMi improves the image quality and the quantitative accuracy of radioactivity distribution determination. Attenuation correction also improves the probability of detecting small and early breast tumors.

Key words: breast PET, attenuation correction, region growing, image segmentation

PACS: 87.57.uk, 87.57.U-, 87.57.nm **DOI:** 10.1088/1674-1137/39/10/108202

1 Introduction

Semi-quantification of radiotracer uptake is useful for nuclear medicine physicians to differentiate benign and malignant tissues. Positron emission tomography (PET) has a reputation for semi-quantitative analysis with an accurate and precise radiotracer concentration map of the whole body. However, the exact activity map is not so easy to achieve and there are many factors to consider, such as photon attenuation, count-rate loss due to dead time, variations in detector efficiency etc. [1]. Of these, most effects have been corrected for the development of PET technology. For example, a generic protocol for attenuation corrections (AC) is combined PET with a transmission scan, such as a rod source or computed tomography (CT) [2, 3]. Nevertheless, attenuation correction is still a challenge in a transmission-less whole-body (WB) PET systems. Since the WB PET detects a complicated and comprehensive radiotracer distribution image consisting of bone, air, soft tissue and other components, it makes precise image segmentation from the activity map difficult.

In recent years there has been a boom in developing organ-dedicated nuclear medicine techniques. Among these systems, positron emission mammography has achieved the fastest development. With a small and compact detector, positron emission mammography has good resolution and image quality [4–6]. A new polygon Positron Emission Mammography imaging system called PEMi, with the ability to detect millimeter-sized lesions, was developed in 2009 by the Institute of High Energy Physics, Chinese Academy of Sciences. It is capable of producing breast-PET images with better quality than standard methods [7]. The generic protocol for AC in PEMi uses an image segmentation method. We take advantage of the simple structure of the breast. The radiotracer distribution of the breast is clear and simple, which makes an AC method based on image segmentation easy and practical in PEMi.

AC methods in transmission-less PET systems have been studied for many years. Early approaches to AC methods started with the pioneering work by Censor et al. They used an iterative algorithm to extract the activity map and attenuation map out of emission data

Received 18 December 2014, Revised 15 June 2015
∗ Supported by Knowledge Innovation Project of The Chinese Academy of Sciences (KJCX2-EW-N06)
1) E-mail: guxiaoyue@ihep.ac.cn

simultaneously [8]. A major limitation, however, is the inherent cross-talk between the two maps, which makes the method impractical for clinical applications. Natterer et al. proposed a more popular approach to estimate the attenuation map based on the data consistency conditions (DDCs) [9]. The DDCs method has already been tested in the PEMi system. It is powerful in most situations, but if the activity distribution of the cancer lesion is more concentrated than the breast tissues, it will only give the breast tumors as the segmentation result. It is also impossible to segment the breast tissue from the background regions [10]. Manual boundary modification is easy to perform but it has the major disadvantage of being time-consuming for applications.

The well-known seeded region growing (SRG) algorithm is a powerful and flexible approach for image segmentation [11]. It performs well in searches of homogeneous regions inside the image based on connectivity and similarity properties among the voxels. The basic process of SRG starts from an initial set of voxels, known as the "seeds". The nearby voxels are then selected according to certain predefined criteria. The method is robust, rapid, and free of tuning parameters, however it is sensitive to noise. The development of the SRG method in three dimensions (3D) has already been studied and applied in other clinical imaging methods, such as CT and MRI [12–14].

In this study, a method is proposed to perform attenuation correction with a 3D seeded region growing (3DSRG-AC) image segmentation algorithm. The 3DSRG method gives a 3D connected region as the segmentation result instead of two-dimensional (2D) image slices. The 3D connective property makes the method free of concentration variations between image slices, and all the breast tissues including both normal tissues and lesions are segmented as a whole. The watershed value between the breast tissues and the air region is chosen as the threshold for region growing, which works fine in the differentiation process. The key point of this method is a prior Gaussian filter application and setting the first valley of the grey level histogram of the image as the lower threshold of the region growing method. We have tested the method with experimental data and clinical data from PEMi, and have achieved stable and robust results. The dedicated breast PET was made by the Institute of High Energy Physics, Chinese Academy of Sciences [7].

2 Methods

2.1 System design

The PEMi detector is designed in a polygon structure, constructed with 16 modules. These modules link in the shape of a detector ring, as shown in Fig. 1(a). Each module consists of four blocks, and each block has 16×16 crystal arrays with a pixel size of 1.9 mm× 1.9 mm×15 mm. The crystals are made of cerium-doped LYSO. To improve light transmission, the top surface of each crystal is roughened, and the other sides (the four sides around and the side coupled to the PSPMT) are optically polished. An enhanced specular reflector is used between the crystal elements to reduce optical crosstalk.

A position-sensitive photomultiplier tube (PS-PMT, Hamamatsu R8900-C12) is coupled to the end face of the scintillator arrays with a tapered light guide, as shown in Fig. 1(c). The specially designed light guide is made of optical fiber to ensure high light transmission, thus linking the scintillator array (32 mm×32 mm) and the PMT (23.5 mm×23.5 mm). The module design is shown in Fig. 1(b). The pixel map of one detector has been obtained (see Fig. 2(a)). All the 16×16 crystals are clearly identifiable in the flood histogram. The associated profiles are also shown in the figure (see Fig. 2(b))

Fig. 1. (color online) Detector design. (a) Photograph of the PEMi detector ring. (b) Photograph of a PEMi module. (c) Schematic of the PEMi block.

Analog signals from the PSPMT are first processed in the front-end electronics. The resistor chains reduce the $6(X)+6(Y)$ anode signals from each PSPMT into four channel signals. The timing signals are acquired from the PMT's last dynode, processed by the constant fraction discriminator, and then transmitted to the data acquisition electronics system together with the processed analog signals.

The axial FOV spans 128 mm, whereas the transaxial FOV is restricted to a diameter of 110 mm by the software after list-mode acquisition. The system operates in full 3D acquisition mode, permitting coincidences between any two detector rings. Both the list mode and histogram mode are provided in the acquisition process. In the histogram mode, coincidence event data are sorted into sinograms and converted into 2D slice data by single slice rebinning (SSRB) [15] and Fourier rebinning (FORE) [16] algorithms using different span and ring differences. Images are reconstructed with a pixel size of 0.5 mm×0.5 mm in a matrix of 256×256. The 2D

filtered back projection (FBP) [17] algorithm or the 2D ordered subsets expectation maximization (OSEM) [18] algorithm can be chosen through user interface. The 3D Gaussian post-filter is optional in the reconstruction process to reduce image noise. The reconstructed images are then displayed in 3D mode and the sagittal, coronal, and transverse views are provided [7].

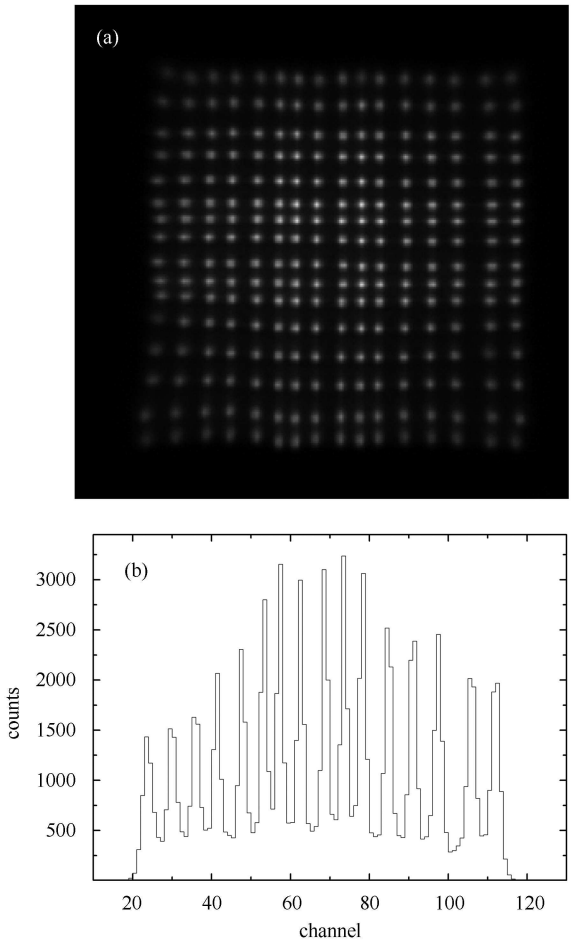

Fig. 2. Detector performance. (a) A pixel map from one detector's arrays shows good detector element separation; (b) Profiles of center channel of the flood histogram.

2.2 Attenuation correction with region growing method

A flow chart of the 3DSRG-AC algorithm is presented in Fig. 3. First time reconstruction of the sinogram is performed before image segmentation, then the reconstructed PEMi image is segmented by the 3DSRG method. Siddon ray tracer projection is processed on the segmentation result to obtain AC coefficients for each line of coincidences (LOR) in the sinogram. In addition, the LORs in the sinogram are multiplied with the AC coefficients for each. With procedures mentioned above, AC has already been performed in PEMi. However in order to obtain the attenuation corrected PEMi image, the image reconstruction process has to be performed again.

The key procedure of the 3DSRG-AC algorithm is the segmentation step. Segmentation starts from an initial set of voxels, known as "seeds". The nearby voxels are then grouped into the growing region when they meet the predefined criteria. Whenever a new voxel is involved in the growing region, a new round traverse over its neighborhoods starts. The iterative process stops when all voxels have been traversed or no voxel meets the predefined criteria. The predefined parameters are set as follows in 3DSRG-AC:

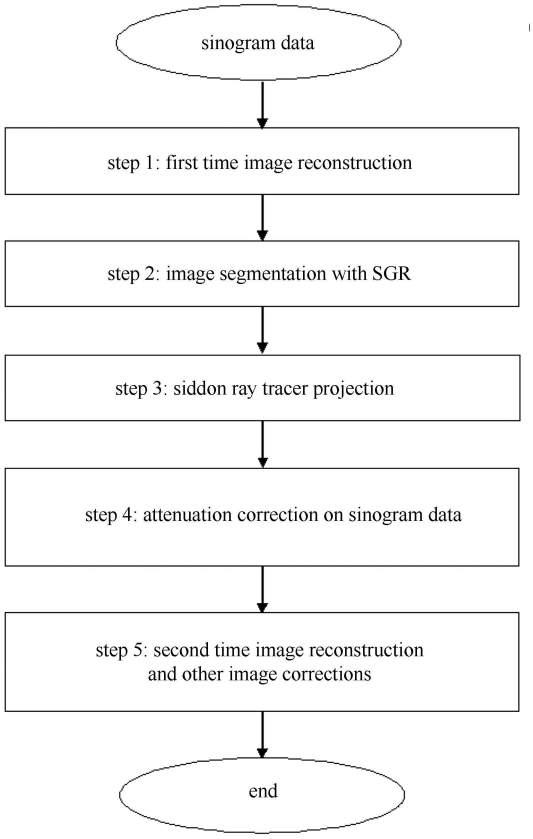

Fig. 3. Flow chart of the 3DSRG-AC algorithm.

Seeds: Maximum value of the PEMi image is chosen as the growing seed for the algorithm;

Growing criteria: The lower threshold of the interval is chosen as the first valley of the grey level histogram after a Gaussian filter application for the PEMi image, see the red triangle mark in Fig. 4; the upper threshold is chosen as the maximum value of the image;

Stop criterion: no voxel meets the growing criteria.

Sixteen neighborhoods are chosen in the 3DSRG-AC method for the 3D growing process, which is effective and fast (see Fig. 5). The breast tissues are separated from the air based on the specified threshold in step two of the

flow chart. Then different attenuation coefficients (ACs) are assigned to breast and air regions respectively. The coefficients of the breast and air regions are as follows [19]:

$$\mu_{\rm breast} = 0.0096\ {\rm mm}^{-1}, \quad (1)$$

$$\mu_{\rm air} = 1.04\times10^{-5}\ {\rm mm}^{-1}. \quad (2)$$

To obtain the attenuation matrix, the PEMi image values are reset in accord with the segment result. Each LOR gets the attenuation coefficient from the attenuation matrix projection. In step three, the Siddon ray tracer is applied for the projection process [20]. The reconstruction process is performed again with the attenuation corrected LORs. The LOR coefficients are obtained as follows:

$$AC_{\rm LOR}=\exp(\mu_{\rm breast}\cdot L_{\rm breast})\cdot\exp(\mu_{\rm air}\cdot L_{\rm air}). \quad (3)$$

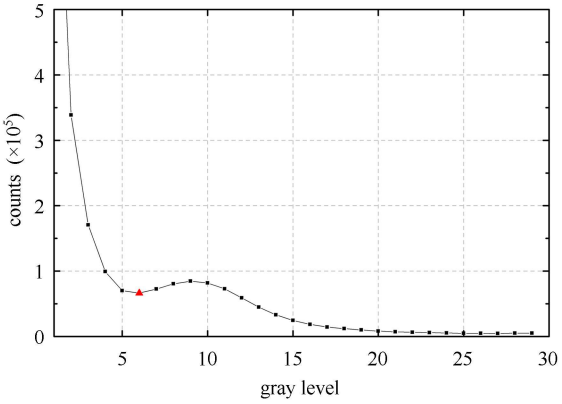

Fig. 4. (color online) Gray level histogram of the PEMi image. The red triangle mark shows the first valley of the grey level histogram of the PEMi image, which is set as the lower threshold.

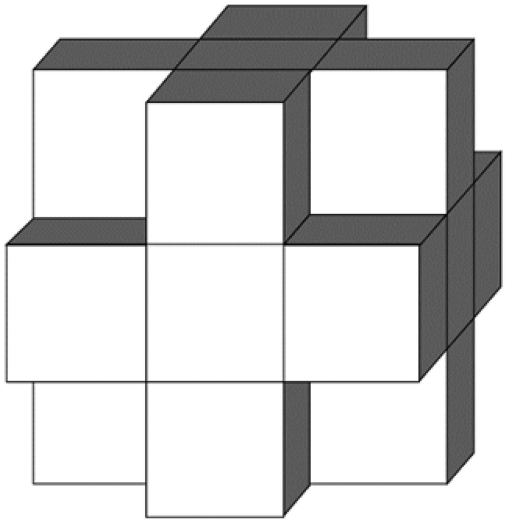

Fig. 5. Neighborhoods for the 3D growing process.

3 Results

3.1 Simulation experiments

We have tested the 3DSRG-AC method by Monte Carlo simulations. Two cylindrical phantoms, both with external diameter of 100 mm and axial height of 157 mm, were employed (see Fig. 6). One of the phantoms was filled with uniform 18F-FDG solution with activity concentration of 200 nCi/cm^3. The other phantom was similar but with four small spherical sources of different diameters, respectively 4 mm, 3 mm, 2 mm and 1.5 mm. All the PEMi data were reconstructed with the OSEM algorithm with two iterations and eight subsets. The attenuation-corrected and uncorrected pictures were both produced with a Gaussian filter.

3.1.1 Uniform phantom

Figure 7 shows the reconstructed results of the uniform phantom. The attenuation-corrected image is more uniform than the uncorrected one. Activity of the uncorrected image declines from the phantom margin to the center. For a detailed quantitative analysis of the results, annular regions of interest (ROI) with 10 mm width were analyzed, as shown in Fig. 8(a). Quantitative analysis of the results is shown in Fig. 8(b).

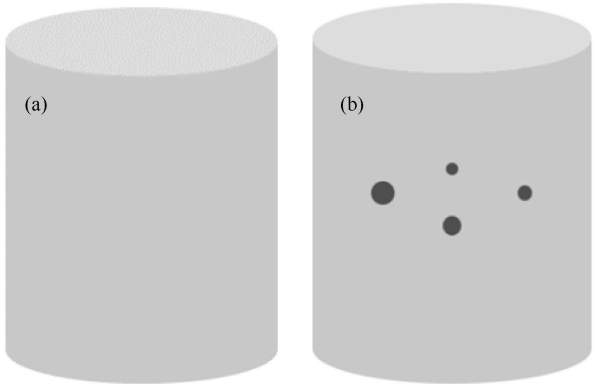

Fig. 6. Phantoms used for Monte Carlo simulation. (a) Uniform phantom; (b) Point Source phantom.

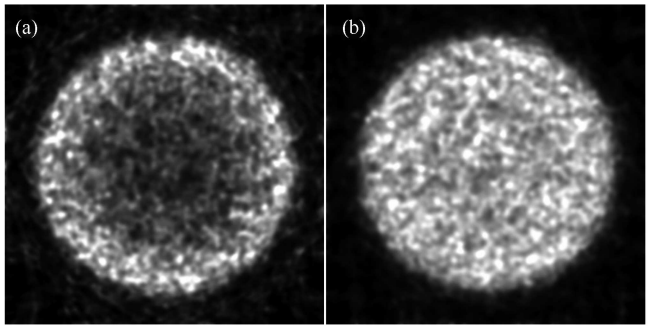

Fig. 7. Reconstructed result of uncorrected view and corrected view. (a) Uncorrected result; (b) Corrected result.

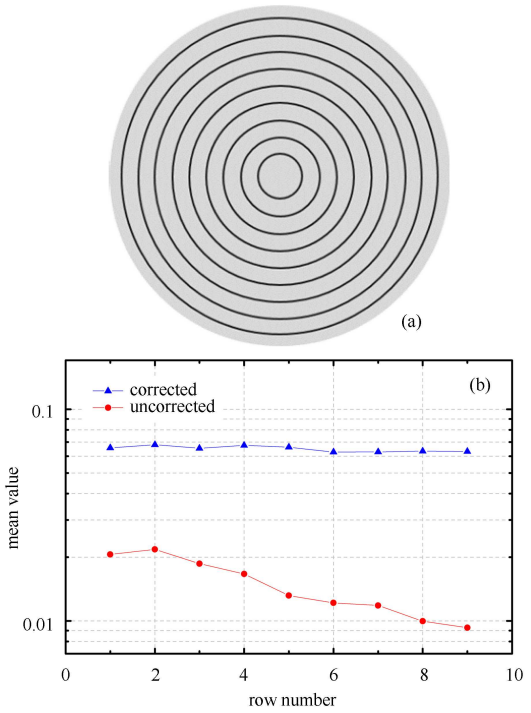

Fig. 8. (color online) Quantitative analysis of uncorrected view and corrected view. (a) Schematic diagram of the ROIs; (b) Quantitative analysis result of the uncorrected and corrected views.

3.1.2 Point source phantom

With the same geometry, the uniform phantom with four point sources was also tested. The reconstructed and attenuation correction methods were the same as the uniform phantom. The maximum intensity projection (MIP) view and transverse views of the results are shown in Fig. 9. The uncorrected image may render a wrong result for the activity distribution, but the corrected image shows greater contrast for the source sites.

3.2 Clinical result

Clinical data were tested with the 3DSRG-AC method. Three views of the segmentation result are shown in Fig. 10. MIP views of the clinical results are given in Fig. 11. Decay, dead time, random, normalization and scatter corrections were all performed for the clinical image. The corrected PEMi data show two lesions of the breast, which were confirmed as an intraductal carcinoma by pathology. There are several suspicious hypermetabolic foci left in this case, shown by the red arrows in Fig. 11. The enhanced uptake is probably due to either inflammation or FDG-avid cancer cells present in the duct. The corrected image shows more details than the uncorrected one, and has better contrast.

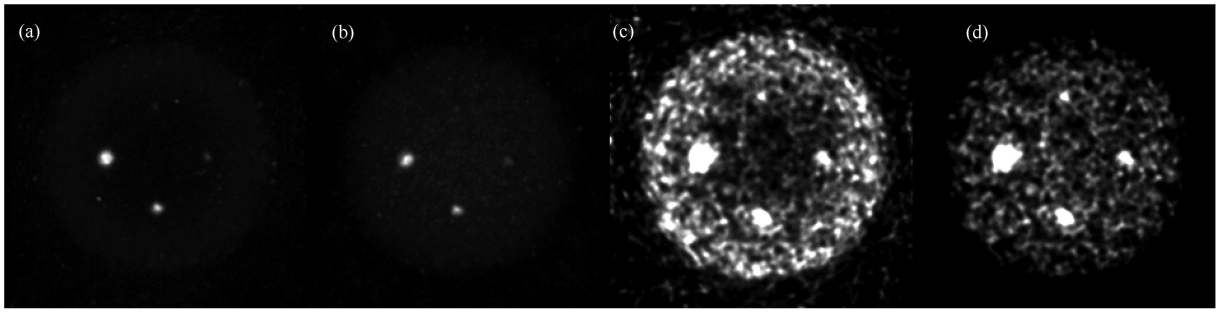

Fig. 9. MIP views and transverse views of the reconstructed uncorrected and corrected pictures of point source phantom. (a) MIP view of the uncorrected result; (b) MIP view of the corrected result; (c) Transaxial view of the uncorrected result; (d) Transaxial view of the corrected result.

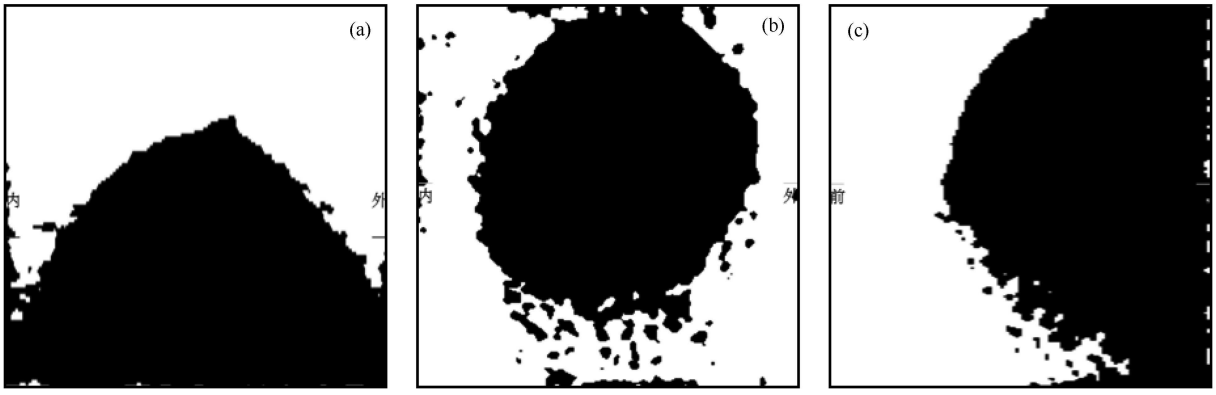

Fig. 10. Segment results of clinical data. (a) Transverse view; (b) Coronal view; (c) Sagittal view.

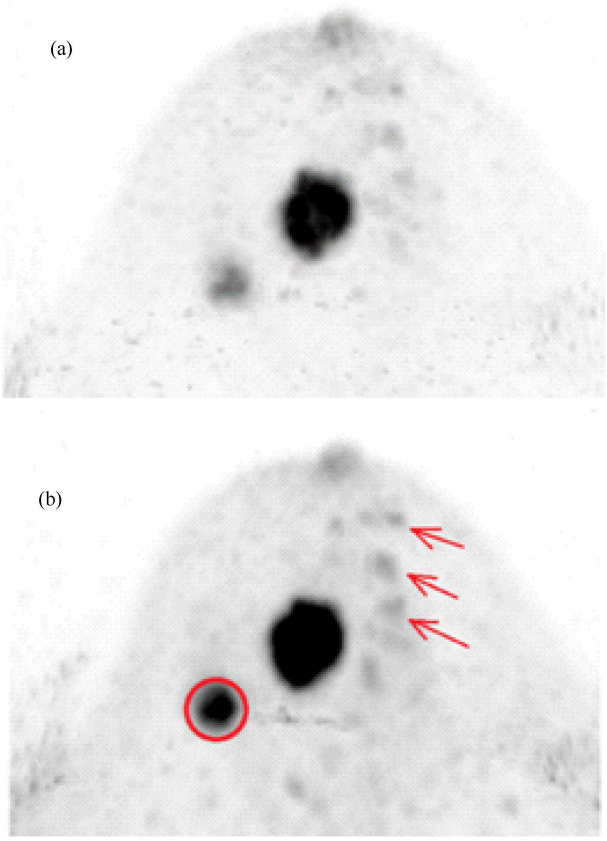

Fig. 11. (color online) Reconstruction result of clinical data. (a) Uncorrected MIP view shows two main lesions; (b) The small lesion in the corrected MIP view is clearer than in the uncorrected view, as are several suspicious abnormal lesions.

4 Discussion

We have developed a new attenuation correction method based on a 3D region growing algorithm, namely 3DSRG-AC. The greatest advantage of the 3DSRG-AC method is that it gives a connected region as a segmentation result instead of 2D image slices. This 3D segmentation property makes use of the advantage of consecutive activity distribution in the breast tissues, which makes the algorithm free of concentration variations between image slices. As a result, the breast tissues including both normal tissue and lesions are segmented as a whole based on their gray level distribution. The slice-by-slice 2D segmentation method easily leads to inconsistent results between slices, typically caused by the different activity distribution between normal tissue and lesions. When the lesions are too concentrated, the 3DSRG-AC method will avoid taking the lesion boundary as the contour.

The 3DSRG-AC method obtains a stable and accurate segmentation result. The threshold value chosen is the key point for the segmentation process. An inappropriate choice of threshold value will render an inaccurate result. For example, the first valley of the grey level histogram of the point source phantom is tested as 10, which is the optimal estimated value of the threshold between breast tissues and air, see the red triangle mark in Fig. 12. With a proper value as the lower threshold to perform AC, an appropriate result can be obtained, see Fig. 13(a)–(c). Using the half value of the proper threshold as the new segment parameter, the tested results show burrs on the contour edges. The half value of the threshold is located in the air domain (see the blue diamond mark in Fig. 12). The burrs on the contour edge would contribute to the excessive attenuation correction and result in lower contrast for the smallest hot point source, see Fig. 13.

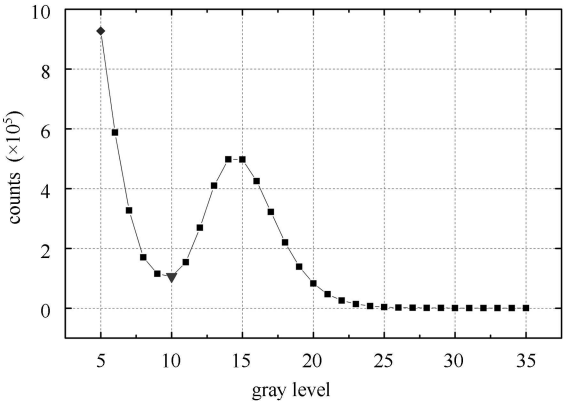

Fig. 12. (color online) Gray level histogram of the PEMi image. The red triangle mark show the optimal threshold. The blue diamond mark show the half value of the proper threshold.

A lower threshold adds noise information to the segmentation image. A more aggressive attenuation coefficient contributed from extra noise information in the segmentation result will further reduce noise interference as well as other activity information. Therefore, we confirm that an appropriate segmentation shape adapted for real phantom or breast tissues is accurate, while excessive attenuation correction will result in the loss of useful information. In practice, we use the first valley of the grey level histogram as the lower threshold, which works fine in clinical application.

As a dedicated-organ imaging system, PEMi is more compact than WB PET, and the gamma ray decay effect in PEMi is less than in WB PET. The phantom data and clinical data show that attenuation correction for PEMi is still important, however. Fig. 8(b) shows the activity profiles drop as depth in the uniform phantom increases in an uncorrected image. The uniform phantom achieves a more uniform result after attenuation correction. This

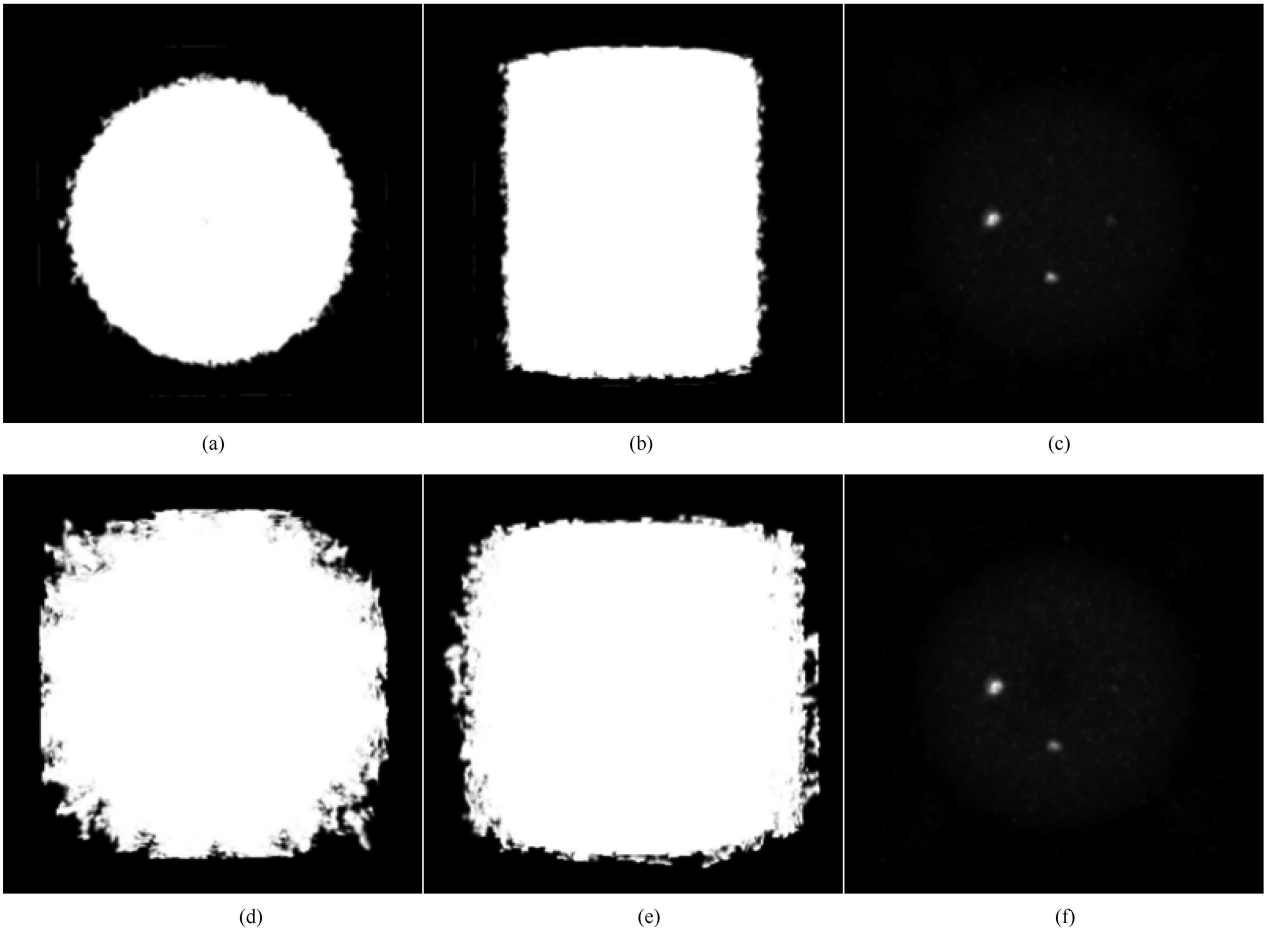

Fig. 13. Comparison of different segmentation thresholds. (a) Transverse view of the proper threshold segmentation result; (b) Sagittal view of the proper threshold segmentation result; (c) Reconstructed result after AC of the proper threshold segmentation result; (d) Transverse view of the low threshold segmentation result; (e) Sagittal view of the low threshold segmentation result; (f) Reconstructed result after AC of the low threshold segmentation result.

effect will affect small lesion detection in the marginal area. As shown in Fig. 9, it is somewhat difficult to distinguish the smallest source from the noise, while the small site can be distinguished in the AC performed image.

In the clinical data shown in Fig. 11, the corrected view shows more information than the uncorrected one, and obtains better contrast for the activity distribution. We take the opinion that attenuation correction makes a contribution to accurate image quality as well as semi-quantification in PEMi.

5 Conclusion

PEMi system provides a novel nuclear medicine diagnosis method dedicated for breast imaging. It has a better resolution in detection of millimeter-sized breast tumors. With a spatial resolution of approximately 2 mm, the PEMi system is capable of producing better quality breast-PET images compared to other nuclear imaging methods. The AC method is based on a 3D region growing algorithm, namely 3DSRG-AC. The greatest advantage of 3DSRG-AC method is that it gives a connected region as a segmentation result instead of 2D image slices. The continuity property of the segmentation result makes this new method free of activity variation of breast tissues. The method also ensures a stable and accurate segmentation result. 3DSRG-AC improves the probability of detecting small and early breast tumors. Results show that attenuation correction for PEMi improves the image quality and the quantitative accuracy of radioactivity distribution determination.

References

1 Valk P E. Positron Emission Tomography: Basic Sciences. Springer Science & Business Media., 2003. 93
2 Beyer T, Townsend D W, Brun T, Kinahan P E et al. J NUCL MED, 2000, **41**(8): 1369–1379
3 Kinahan P, Townsend D, Beyer T et al. MED PHYS, 1998, **25**(10): 2046–2053
4 Abreu M C, Aguiar J D, Almeida F G et al. IEEE T NUCL SCI, 2006, **53**(1): 71–77
5 Moliner L, Gonzalez A, Soriano et al. MED PHYS, 2012, **39**(9): 5393–5404
6 LU X, Anashkin E, Matthews C G et al. Real-time Viewer for Positron Emission Mammography Image-Guided Intervention. Proc. of the 2008 Nuclear Science Symposium Conference Record, 2008. 4814–4819
7 LI Lin, GU Xiao-Yue, LI Dao-Wu et al. Ability of the Positron Emission Mammography System, PEMi, in Detection of Millimeter-Sized Lesions. Proc. of the 2013 Nuclear Science Symposium and Medical Imaging Conference Record (NSS/MIC), 2013
8 Krol A, Bowsher J E, Manglos S H et al. IEEE Trans Med Imaging, 2001, **20**(3): 218–232
9 Natterer F. Determination of Tissue Attenuation in Emission Tomography of Optically Dense Media. Inverse Problems, 1993, **9**(6): 731
10 WANG Lu, CHAI Pei, WU Li-Wei et al. CPC, 2013, **37**(1): 018201
11 Adams R, Bischof L. TPAMI, 1994, **16**(6): 641–647
12 SHEN Yi, WANG Bo-Liang, JU Ying et al. Proc. In: Engineering in Medicine and Biology Society, 2005 IEEE-EMBS 2005 27th Annual International Conference of the: 2006: IEEE; 2006. 2902–2905
13 HUANG Zhan-Peng, YI Fa-Ling, JIANG Shi-Zhong et al. The Segmentation of Liver and Vessels in CT Images using 3D Hierarchical Seeded Region Growing. Proc. of the Computer Science and Automation Engineering (CSAE), IEEE International Conference on, 2011. 264
14 del Fresno M, Vénere M, Clausse A. CMIG, 2009, **33**(5): 369
15 Daube-Witherspoon M E, Muehllehner G. JNM, 1987, **28**(11): 1717
16 Defrise M, Kinahan PE, Townsend DW et al. TMI, **16**(2): 145
17 Chesler D, Riederer S. PMB, 1975, **20**(4): 632
18 Hudson H M, Larkin R S. TMI, 1994, **13**(4): 601
19 White D, Booz J, Griffith R et al. Tissue Substitutes in Radiation Dosimetry and Measurement. ICRU Report 1989, 44
20 Siddon R L. MP, 1985, **12**(2): 252